Calculation of Ce^- binding energies by analysis of photodetachment partial cross sections

Steven M. O'Malley and Donald R. Beck
Physics Department, Michigan Technological University, Houghton, Michigan 49931, USA
(Received 2 August 2006; published 17 October 2006)

The electron affinity of cerium is determined from relativistic configuration interaction photodetachment calculations through a reinterpretation of available experimental data [V. T. Davis and J. S. Thompson, Phys. Rev. Lett. **88**, 073003 (2002)]. This analysis yields a $4f5d^26s^2\ ^4H_{7/2}$ Ce^- ground state (a $5d$ attachment relative to the $4f5d6s^2\ ^1G_4$ neutral Ce ground state) with binding energy of 0.660 eV as well as 18 other bound states of the same configuration. The lowest-lying state of seven bound states of the opposite parity ($6p$ attachments) is $4f5d6s^26p\ ^2H_{9/2}$, which is bound by 0.300 eV.

DOI: 10.1103/PhysRevA.74.042509 PACS number(s): 32.10.Hq, 31.25.Jf, 32.80.Gc, 32.70.Cs

I. INTRODUCTION

By the early 1990s, accelerator mass spectrometry (AMS) experiments such as those by Garwan *et al.* [1] had detected the negative ion of cerium, as well as many other lanthanides [1,2]. The high yield for Ce^- [1] suggested a large electron affinity (>0.6 eV) or several moderately bound states. Density functional theory calculations [3] at the time suggested that rare-earth negative ions are formed by p and possibly d attachments rather than f attachments as previously expected.

In 1994 our group undertook relativistic configuration interaction (RCI) calculations [4] which explored both $6p$ and $5d$ attachments to the $4f5d6s^2\ ^1G_4$ Ce ground state. The latter were actually treated as $6s$ attachments to an excited $4f5d^26s\ ^5H_3$ threshold (the lowest lying of this configuration [5]) due to the greater difficulty of properly correlating negative-ion states and neutral thresholds with differing d occupation (correlation involving differing s occupation has less absolute and differential contribution to energies). This early RCI work [4] predicted an even $J=9/2$ $6p$ attachment to the Ce ground state with an electron affinity of 0.259 eV, four other bound excited even states, and a single odd $5d$ attachment with a binding energy of 0.178 eV.

By the late 1990s, experiments by Berkovits *et al.* [6] involving a combination of laser excitation and AMS techniques had identified the electron affinity of Ce as 0.700 ± 0.010 eV [6]. This value, however, was predicated on the earlier RCI [4] prediction that the ground state of Ce^- was formed by $6p$ attachment.

In 2000, encouraged by a resurgence of experimental interest in rare-earth negative ions [7] and improvements in our own RCI methodology made during our then recent work on La^- [8], we undertook a second set of calculations of Ce^- binding energies [9]. Two main improvements to the methodology over the previous RCI calculations [4] were made at this time. There was extensive inclusion of second-order correlation effects (triple and quadruple replacements with respect to the configurations of interest) which more properly treated key single and double replacements in the Ce^- basis sets and increased binding relative to the neutral Ce states by ~0.090 eV. Also, a higher neutral threshold $4f5d^26s\ ^5I_8$ was chosen for the odd Ce^- $6s$ attachments ($5d$ with respect to the ground state). The choice of $J>6$ for this threshold eliminated difficulties of properly positioning the $4f5d6s^2$ and $4f5d^26s$ manifolds relative to one another in the neutral RCI calculation and moving further to $J>7$ also removed complications of mixing with other nearby $4f5d^26s$ levels [5]. This newer work [9] predicted a $4f5d^26s^2\ ^4H_{7/2}$ Ce^- ground state with electron affinity of 0.428 eV, six other odd bound states, and eight even $4f5d6s^26p$ states with the lowest ($^2H_{9/2}$) bound by 0.349 eV.

In 2002 Davis and Thompson [10] presented laser photodetachment electron spectroscopy (LPES) measurements which determined the electron affinity of Ce to be 0.955 ± 0.026 eV. Their analysis also indicated at least two bound excited states with binding energies of 0.921 ± 0.025 eV and 0.819 ± 0.027 eV [10], all considerably larger than the previous experiments [1,6] and calculations [4,9]. The data for this experiment exhibit three large features in the photoelectron kinetic energy spectrum, and the analysis of these data relies on the assumption that the largest of these features (which also has the highest electron energy of the three peaks) represents the ground-state to ground-state photodetachment channel [10].

Finally, in 2004 Cao and Dolg [11] presented Ce^- calculations using the relativistic energy-consistent small-core pseudopotential methodology. These results also predicted an odd $4f5d^26s^2\ ^4H_{7/2}$ ground state, but their electron affinity for this state was 0.530 eV [11], 0.102 eV more bound than our second RCI Ce^- study [9].

With an aim to resolve the discrepancy of over 0.400 eV among the various calculations and experiments, we once again decided to undertake an RCI study of Ce^-. In preparation for the work presented here we improved our 2000 calculations [9] by considering correlation involving core electrons. Our previous work [4,9] was limited by a basis set maximum of 7000 functions, and the code had since been improved to allow 20000 basis functions. This allowed us to consider correlation involving the singly occupied $4f$ subshell, which had previously been omitted since the small $\langle r\rangle\approx1.1$ a.u. (compared to the $5d\langle r\rangle\approx3.1$ a.u.) suggested this electron could be considered core like and isolated from the valence electrons. An important consideration for the odd states, however, is that $4f6s$ pair replacements contribute approximately twice as much correlation energy to the negative ion ($6s^2$ vs $6s$ in the neutral threshold), and because there is only a single $4f$ electron present, there are no replacements of the form $4f^2\rightarrow6snl+6svl$ (nl here representing $5d$ and vl representing any subshell not occupied in the ground-state

configuration), which would tend to offset this difference with a larger contribution to the neutral correlation energy. The electron affinity of Ce^- was thus increased from our previous 0.428 eV [9] to 0.511 eV, in good agreement with the other calculation [11].

Further test calculations suggested more binding could be obtained through opening the $5p$ subshell, but the amount of correlation ($\sim$3–4 eV for a differential contribution of $\sim$0.100 eV) prohibited inclusion of this core-core and core-valence correlation, since doing so would disrupt the position of the ground-state configurations relative to the valence correlation configurations (resulting in losses of the valence correlation of approximately the same size as the amount of differential core correlation we were attempting to introduce).

At this stage we decided to approach the calculation of the Ce^- binding energies from a different direction, using RCI calculations of photodetachment partial cross sections to identify the dominant photodetachment channels and comparing these results with published experimental data [10]. This reduces the usual concerns of a careful treatment of the equivalent correlation in the negative-ion and neutral RCI calculations (as exhibited by our need to select the excited-state threshold to eliminate the problem of differing $5d$ occupation), and it also utilizes precise energy measurements of the experimental data [10] (with the key being a revised identification of the prominent features of the experimental photoelectron energy spectrum).

Our revised interpretation of the experimental data [10] is largely based on the realization that, considering dominant LS terms, the ground-state to ground-state channel in Ce^- represents a forbidden transition due to differing total spin (the negative ion is a quartet state and the neutral singlet threshold plus photoelectron can only make a doublet state). There is, however, an additional consideration that the Ce^- $6s$ one-electron radial function is much more diffuse than the $5d$ radial function (the average r is over twice as large). This may have larger implications for many other lanthanide negative ions with ground-state configurations of the form $4f^m5d^n6s^2$, regardless of the LS term, because a $6s \rightarrow \epsilon l$ channel to an excited $4f^m5d^n6s$ threshold may have a much larger partial cross section than a $5d \rightarrow \epsilon l$ channel to the $4f^m5d^{n-1}6s^2$ ground state (all neutral lanthanide ground states contain a $6s^2$ subgroup [5]). Depending on the position of the excited $4f^m5d^n6s$ threshold, an assumption that the dominant feature of a photoelectron kinetic energy spectrum represents the ground-state to ground-state channel may overestimate the electron affinity by several tenths of an eV. Given this possibility, we suggest that the Ce^- work presented here may be a model for future comparison between experimental measurement and computational analysis, and it may serve to explain several recent measurements of lanthanide electron affinities $\sim$1 eV—e.g., [12–14]—which are difficult to support theoretically. Since most lanthanides likely have bound states (and perhaps ground states) formed by $6p$ attachments—i.e., $4f^m5d^{n-1}6s^26p$—which would have large partial cross sections to the ground state (of the form $6p \rightarrow \epsilon l$), experimental information regarding the parity and l of the emitted electrons for each feature in the experimental spectra would prove useful in this process.

II. COMPUTATIONAL METHODOLOGY

The RCI calculations begin with one-electron basis sets generated from the multiconfigurational Dirac-Fock (MCDF) program of Desclaux [15]. Our multielectron wave functions are then eigenstates of J^2, J_z, and the parity operator. Correlation is included by adding configurations representing all valence single and double replacements from the multielectron MCDF basis (including correlation of the $4f$ electron as mentioned in Sec. I). Subshells not present in the ground-state configurations of Ce and Ce^- are represented by relativistic screened hydrogenic functions, denoted vl (with $l \leqslant 4$). The effective charges Z^*'s of these "virtual" subshells are determined by an energy-minimizing variational procedure. In this case we found two sets of virtual orbitals (vl,vl') adequate to saturate our correlation configurations.

For purposes of analysis of level composition we create LS approximate basis functions for our configurations of interest. While the RCI calculations are fully relativistic, we can rotate the $j-j$ basis set by neglecting the minor components of the one-electron radial functions and treating the $j=l-1/2$ and $j=l+1/2$ radial functions as equivalent. Using these assumptions, diagonalization of the L^2+S^2 matrix results in a new set of basis functions of the same size (i.e., no information is lost) as the original $j-j$ basis.

As mentioned in Sec. I, opening the core ($5s$ and $5p$ subshells) would prove difficult as it introduces several eV of core-core and core-valence correlation to a calculation that has a total correlation of $\sim$1.5 eV at the valence stage, thus disrupting the relative positioning of the valence correlation configurations. For Ce^-, this is not an issue since the odd (even) states are nearly pure $4f5d^26s^2(4f5d6s^26p)$. However, the neutral Ce spectra exhibit a great deal of mixing of the odd $4f5d^26s$ and $4f5d6s^2$ configurations (as well as $4f^25d6s$ and $4f5d6s6p$ mixing in the even cases). Particularly in the odd Ce calculations we found an overall displacement of the $4f5d^26s$ manifold relative to $4f5d6s^2$ of $\sim$0.100 eV (recall that our earlier calculations [9] avoided this issue by utilizing a $J=8$ threshold, removing $4f5d6s^2$ from consideration). In this case we have included limited core correlation by restricting certain subgroups of electrons. For example, the configuration $5p^5vp4f5d^26s$ serves as a single replacement correction to the $5p$ one-electron radial function which has been generated [15] to optimize the $4f5d6s^2$ configuration. By restricting the $5p^5vp$ subgroup to ^1S we avoid the inclusion of basis functions that represent the double replacement $5p6s \rightarrow 5dvp$ in the $4f5d6s^2$ configuration. With this technique the $4f5d^26s$ manifold is differentially lowered $\sim$0.090 eV with just $\sim$0.160 eV total added correlation.

Attention to $4f5d^26s$ and $4f5d6s^2$ mixing in the neutral Ce spectra is critical due to the fact that many of the dominant terms of nearby levels result in alternating allowed or forbidden transitions from our calculated Ce^- states. For example, the primary reason that we believe a reinterpretation of the experimental data [10] is required is that our Ce^- ground state is ^4H, while the combination of the neutral Ce ^1G ground state and a continuum electron can make at most doublet states (recall $\Delta S=0$ for electric-dipole transitions). There is, however, significant ^2G mixing in the Ce^- ground state [9,11] and some ^3H in the neutral level [5], but we

expect some other channels with dominant terms representing allowed transitions to be stronger.

Since our principal goal here is to identify dominant photodetachment channels (and not, for example, accurate calculation of hyperfine structure of neutral Ce levels), we have elected to deviate from a purely *ab initio* approach and further refine our neutral Ce calculations through shifting of individual *LS* terms. Many of the levels in the Ce spectrum are within a few hundred cm^{-1} of nearby levels of the same *J*, and few are *LS* pure to greater than 60%–70% [5]. In order to better reproduce the experimental spectrum [5], we shift individual diagonal elements of our approximate *LS* basis, most by ~0.100 eV or less. The process is a nonlinear one (typically the diagonal shift results in approximately half as much change in individual eigenvalues), and often different combinations of shifts of several terms can produce the same overall *LS* composition of nearby levels. For example, shifting the dominant term of an upper level down or that of a lower level up can result in the same change in mixing of those two levels. In general, however, our shifts are made with two main criteria in mind: each shift is made by as little as possible to achieve the desired result, and whenever possible we attempt to match the experimental Landé *g* value [5] (rather than the semiempirical *LS* analysis [5]) of as many neutral states of a given *J* as possible.

The final states of our photodetachment partial cross sections are created using a frozen-core approximation. The neutral-core portion of each basis function is restricted to the *J* of the corresponding neutral Ce total *J*. This allows us to include all the correlation and shifting of the *LS* terms that we introduced to the neutral calculations by producing a neutral-core plus continuum-electron basis set that has a one-to-one correspondence with the neutral basis set. We then sum over several cross sections representing the same Ce^- initial state and neutral threshold. For example, our early candidate for one of the dominant transitions was $4f5d^26s^2\ ^4H_{7/2} \rightarrow 4f5d^26s\ ^5H_4 + \epsilon p$, whose cross section is a sum over five relativistic channels: three $\epsilon p_{3/2}$ channels with total $J=9/2,7/2,5/2$ and two $\epsilon p_{1/2}$ channels with total $J=9/2,7/2$.

Our current capabilities using this frozen-core approximation, as opposed to, for example, the more rigorous *R*-matrix approach [16,17] used by more established practitioners in the photodetachment field (e.g., [18]), is appropriate in this Ce^- case for several reasons. The most practical issue is the size of the final-state calculation. With the amount of correlation already included in the final-state core with an effective four-valence-electron calculation, we already have 10–15 000 basis functions per neutral *J*. Adequate correlation of five valence electron states with interleaved manifolds in a system as complicated as Ce^- would likely prove too computationally costly, requiring a basis size several times our current 20 000 limit. As we shall show in Sec. III, the photoelectron kinetic energy spectrum of Ce^- is dominated by channels representing $6s \rightarrow \epsilon p$, so a careful treatment of the interchannel coupling between channels with continuum electrons of differing *l* is not required ($5d \rightarrow \epsilon p + \epsilon f$ channels are found to have a negligible impact; see Sec. III). Since we are comparing our results with experimental LPES measurements [10] where the incident photon energy is fixed, rather than the variable photon energy of the laser photodetachment threshold (LPT) method, concerns regarding the possible narrow resonance features present in calculations over a wide range of photon energies [18] are also less immediate. Finally, we consider that our stated goal of these calculations is to determine the dominant photodetachment channels and identify them with the features of the experimental [10] kinetic energy spectrum. Ultimately, our values for the Ce^- binding energies are dependent upon this analysis and use of the experimental energy measurements [5,10], not the precise ratios of various partial cross sections.

Our continuum functions are generated using the relativistic continuum wave solver code of Perger and co-workers [19,20]. Each channel requires a separately generated continuum function with the core determined by the final-state threshold, the structure of the multielectron configuration determined by the final-state threshold and total *J*, and the energy of the continuum function calculated by subtracting the difference of the negative-ion initial-state and neutral threshold from the incident photon energy. The photodetachment code is a modification of our relativistic *f* value code with full treatment of nonorthonormality between the initial- and final-state radial bases. Ultimately, this work resulted in the calculation of over 4000 individual relativistic photodetachment channels, though only a small minority of these play a significant role in the final analysis.

The approach to the comparison with the experimental data [10] took place in three passes. The first set of calculations were made at the MCDF level (little to no correlation) with rough estimates for the photoelectron energies. These were used to select the candidates for channels that corresponded to the dominant features of the experimental spectrum. It was quickly learned that the partial cross sections from the ^4H Ce^- states to the ^5H $4f5d^26s$ neutral Ce thresholds ($6s \rightarrow \epsilon p$) were over an order of magnitude larger than those to the ^1G ground state. Identifying these transitions with the dominant high-energy peak of the experimental spectrum [10] effectively lowered the Davis-Thompson electron affinity by nearly three-tenths of an eV. Once this choice of placement of the Ce^- ground state was made, the second largest feature was identified with a higher ^3H threshold and confirmed by the similar size of the partial cross sections of these channels. The lowest-energy feature could not be identified with any channel with an odd initial state, but using our earlier position of the lowest 6*p* attachment [9] as a guide, channels from the even Ce^- states to $4f5d6s6p$ (also $6s \rightarrow \epsilon p$) were considered and also found to have relatively large cross sections.

With this analysis, the lowest Ce^- state of each parity was approximately placed and all other bound state binding energies were determined by relative position in the RCI negative-ion calculations. Once the detailed partial-cross-section calculations were made, they were combined (as discussed in Sec. III) to produce a simulated kinetic energy spectrum. The final step was to adjust the binding energies to match the peaks in this simulated spectrum with those of the experimental data [10] (−0.003 eV for the odd levels and +0.028 for the even levels) with the assumption that such a small change in the continuum electron energies would not significantly affect the calculated partial cross sections.

TABLE I. Ce^- odd state leading *LS* terms (%), lifetimes, and binding energies (eV) with previous computational results.

$Ce^- 4f5d^26s^2$	τ[a]	RCI	[11]	[9]	[4]
$^4D_{1/2}$ 77, ^2P 21, ^2S 2	∞[b]	0.302			
$^2S_{1/2}$ 45, ^2P 22, ^4D 13	34 ms	0.073			
$^4D_{3/2}$ 92, ^2P 6, ^4F 2	162 s	0.231			
$^4F_{3/2}$ 94, ^2D 5, ^4D 1	80 ms	0.106	0.062		
$^2F_{5/2}$ 56, ^4D 32, ^4G 6	55 s	0.234	0.168		
$^4D_{5/2}$ 55, ^2F 22, ^4G 19	170 ms	0.125	0.018		
$^4F_{5/2}$ 58, ^4G 27, ^4D 9	72 ms	0.054			
$^4H_{7/2}$ 71, ^4G 27, ^2F 1	∞[c]	0.660	0.530	0.428	0.178
$^2G_{7/2}$ 56, ^4H 27, ^2F 13	28 s	0.428	0.332	0.182	
$^2F_{7/2}$ 44, ^4D 36, ^2G 13	416 ms	0.232	0.096		
$^4D_{7/2}$ 39, ^4G 29, ^2F 18		0.008			
$^4H_{9/2}$ 59, ^2G 34, ^2H 4	51 s	0.550	0.421	0.327	
$^4I_{9/2}$ 91, ^2H 5, ^4H 4	403 s	0.508	0.242	0.281	
$^2G_{9/2}$ 60, ^4H 35, ^4F 2	27 s	0.403	0.276	0.167	
$^2H_{9/2}$ 85, ^4I 7, ^2G 5	181 μs	0.126			
$^4H_{11/2}$ 50, ^4I 46, ^2I 4	46 s	0.419	0.229	0.193	
$^4I_{11/2}$ 48, ^4H 46, ^2H 5	16 s	0.380	0.101	0.149	
$^2I_{11/2}$ 91, ^4I 4, ^2H 4		0.020			
$^4H_{13/2}$ 48, ^4I 43, ^2I 9	36 s	0.306	0.084		
$^4I_{13/2}$ 52, ^4H 48	12 s	0.220			
$^4I_{15/2}$ 100	10 s	0.086			

[a]States with $\tau > 1s$ have no $E1$ branches (see Table III).
[b]No single photon $E1$, $M1$ or $E2$ decay is possible.
[c]Ce^- ground state.

III. RESULTS

In Tables I and II, we present the *LS* composition and binding energies of 26 states of Ce^- which are predicted bound by 0.030 eV or more (the typically expected accuracy of relative position of levels within a manifold in our RCI calculations which are not complicated by mixing of two configurations). Two other possible odd states are presented with binding energies of 0.020 and 0.008 meV, although no photodetachment calculations were made involving these levels. Lifetimes presented in these tables are calculated using revised relative positions of the even and odd Ce^- states (increased by ~0.250 from our earlier calculations [9]). Where applicable we use the Babuskin (length) gauge of the $E1$ operator, as we find it is more reliable for smaller f values than the Coulomb (velocity) gauge, which often involves more cancellation in the final correlated value relative to the MCDF value (i.e., it is less stable when considering small changes in the RCI basis set). Many of the odd states have no possible $E1$ branch to a lower even state, resulting in several long-lived ($\tau > 1$ s) excited Ce^- states. In particular, the $^4D^o_{1/2}$ state (lower than the lowest $J=3/2$ and $J=5/2$ states) must decay by some other mechanism than a single-photon transition.

TABLE II. Ce^- even state leading *LS* terms (%), lifetimes, and binding energies (eV) with previous computational results.

$Ce^- 4f5d6s^26p$	τ	RCI	[11]	[9]	[4]
$^2D_{3/2}$ 53, ^4F 33, ^4D 8	713 μs	0.141		0.135	0.043
$^4G_{5/2}$ 54, ^2F 40, ^2D 5	155 μs	0.156	0.080	0.203	0.105
$^2G_{7/2}$ 77, ^4H 9, ^2F 8	154 μs	0.185	0.008	0.215	0.147
$^4H_{7/2}$ 48, ^2G 27, ^2F 17	18 μs	0.083		0.153	0.055
$^2H_{9/2}$ 62, ^4I 18, ^2G 16	336 μs	0.300	0.156	0.349	0.259
$^4I_{9/2}$ 49, ^2G 41, ^4F 5	43 μs	0.045		0.104	
$^2H_{11/2}$ 75, ^4I 17, ^4G 6	102 μs	0.076		0.117	

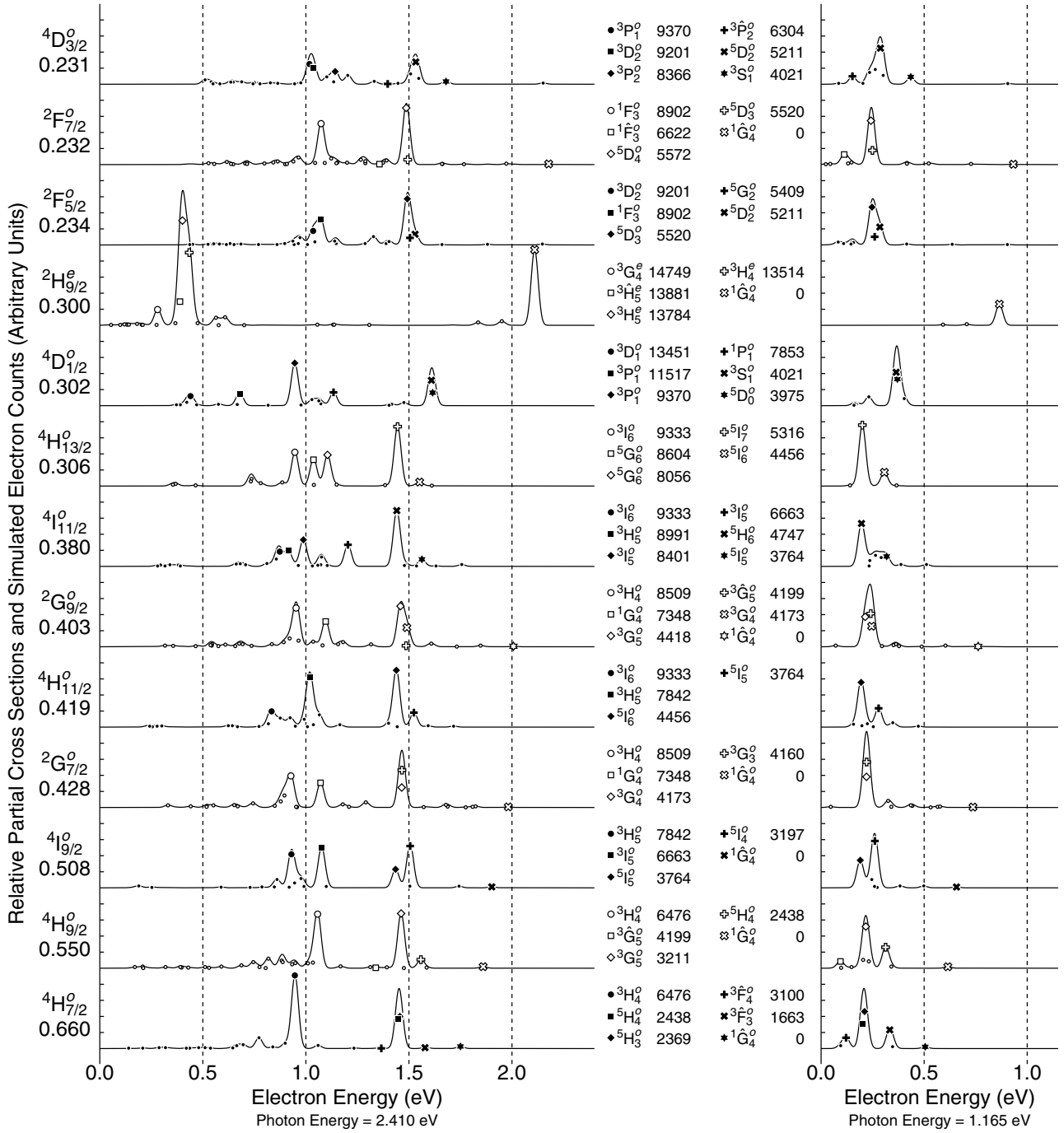

FIG. 1. Simulated electron counts and relative partial cross sections for given Ce^- initial states. The dominant *LS* term and binding energy (in eV) for each odd ($4f5d^26s^2$) or even ($4f5d6s^26p$) Ce^- level appear on the left side of each row. The legend for each row indicates the most important channels by the corresponding neutral Ce threshold (with energy in cm^{-1} [5]), mainly $4f5d^26s(4f5d6s6p)$ for odd (even) levels with the caret in the *LS* term indicating $4f5d6s^2$ ($4f^25d6s$) levels.

In Figs. 1 and 2 we present simulated electron count plots for individual Ce^- initial states for the two photon energies used in the LPES experiment [10]. Also shown are the normalized partial photodetachment cross sections; the cross sections for the 1.165 eV photon energy are ~5.8 times larger, but these data have been adjusted such that the $^4H_{7/2} \rightarrow {}^5H_{3,4}$ peaks are of the same height in both plots (the relative sizes within each photon energy are plotted with a consistent scale, however). Only partial cross sections greater than 1% of the sum of these two channels are shown. The curves are generated by simply adding a Gaussian proportional to the size of each partial cross section at the appropriate electron energy with the constant width chosen to match closely the eventual combined plots (see Figs. 3 and 4) with the experimental data [10].

The final simulated plots in Figs. 3 and 4 are generated by adding the plots of Figs. 1 and 2 with a multiplicative coefficient for each Ce^- initial state based on Boltzmann dis-

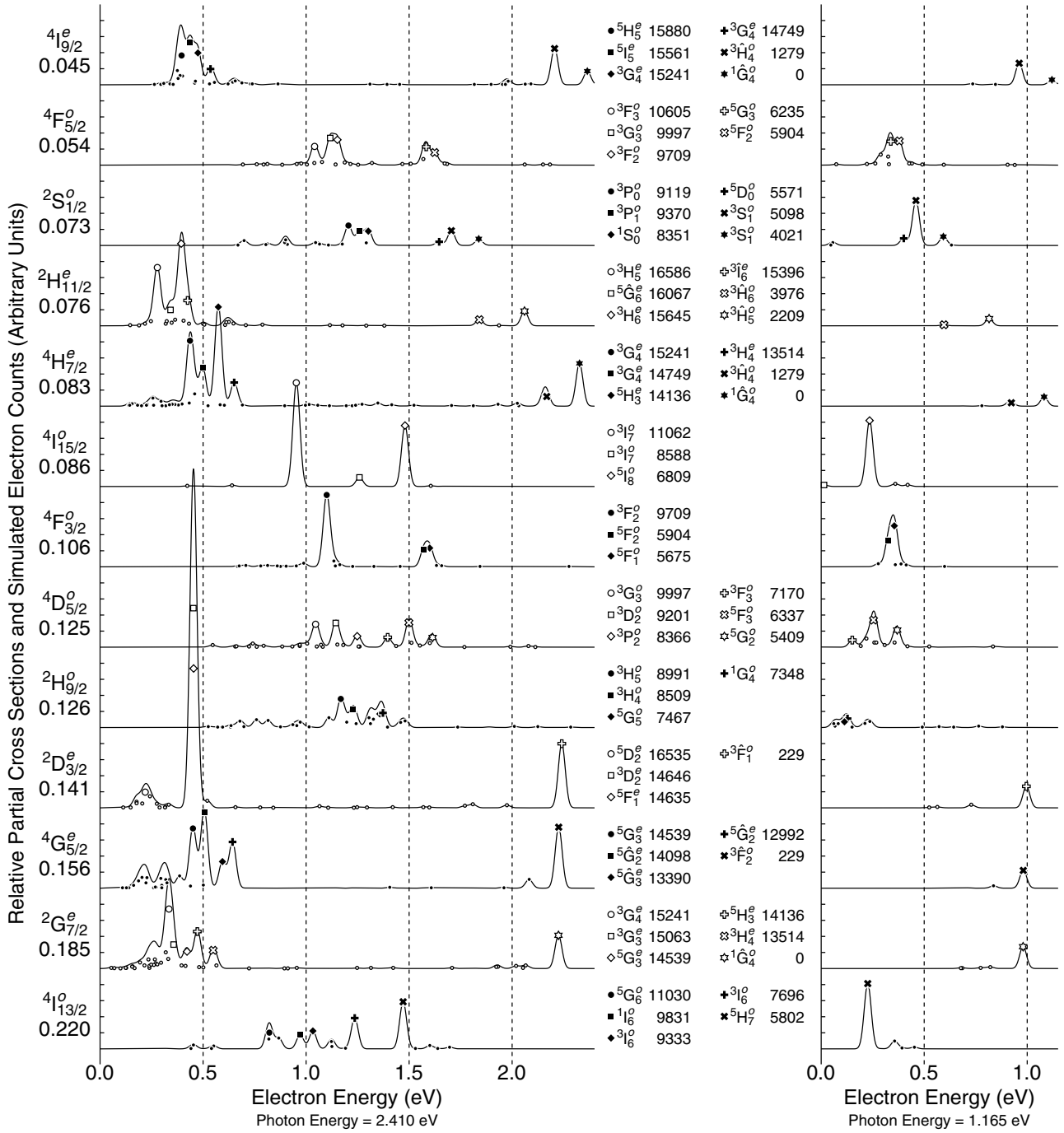

FIG. 2. Simulated electron counts and relative partial cross sections for given Ce^- initial states (continued; see Fig. 1).

tributions with several possible effective temperatures. This is not to say that we are attempting to measure the actual temperature of the ion beam, as the sputtering process used to create the Ce^- ions is a chaotic one and not likely to represent a process in thermal equilibrium. However, a realistic estimate of the relative population of states involving consideration of the interaction with the cesium-sputter negative-ion source and the various components of the target [10], collisional excitations and decays during production (and perhaps within the resultant beam), etc., is beyond the scope of this study and the expertise of its authors.

Redistribution of states due to photodecay or photoexcitation was also considered but expected to be insignificant due to the fact that the majority of the lifetimes in Tables I and II are much longer than the $\sim 50\ \mu s$ [14] time of flight of the experimental apparatus. The fact remains that some distribution needs to be chosen to produce the plots, and the consistency of the general form of the resulting simulated plot (position and dominance of the three main peaks) over a wide range of effective temperatures is a testament to the robustness of this approach. The arbitrary units of the vertical axes of these simulated plots were simply chosen to

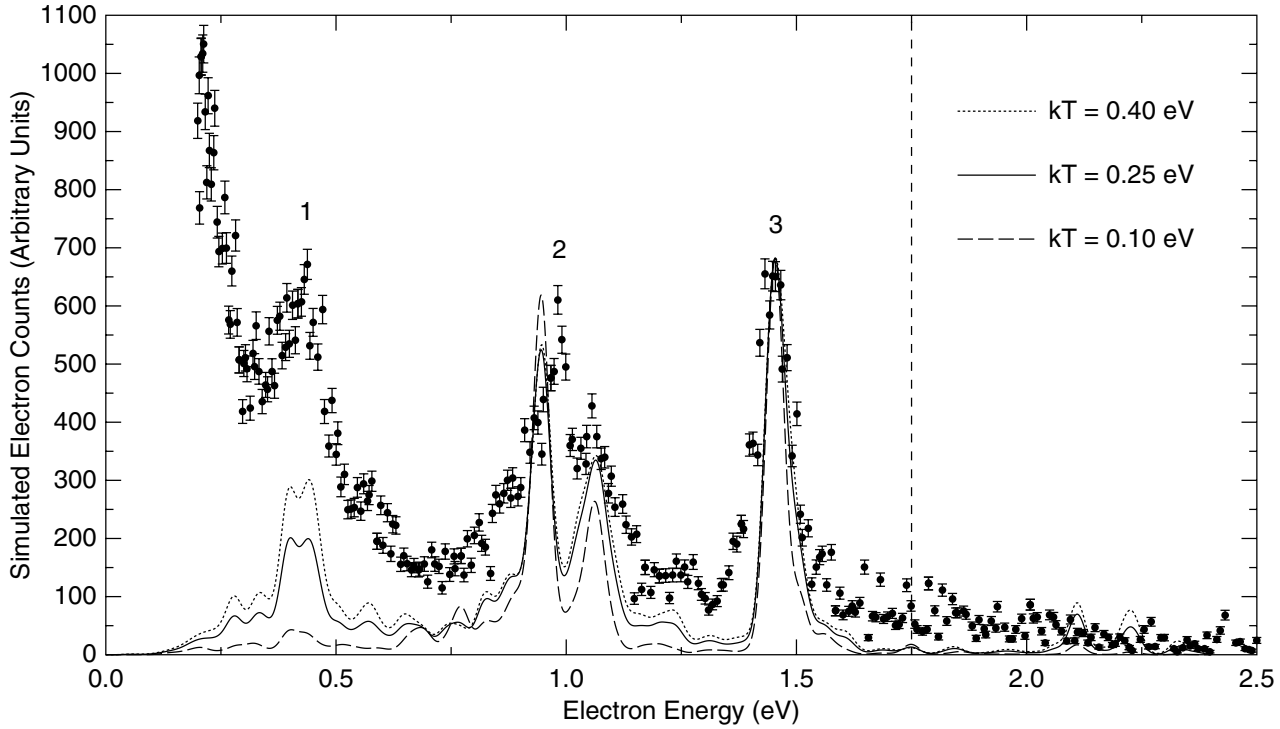

FIG. 3. Simulated electron counts for incident photon energy of 2.410 eV. The points and error bars are the Davis-Thompson [10] experimental results. The dashed vertical line indicates the position of the ground-state to ground-state channel with our revised interpretation. The broad low-energy increase in electron counts in the experimental data is due to "collisional detachment of Ce^- ions in the beam by background gas and ion-aperture scattering" and has not being included in our simulated plots.

match the range presented in the experimental publication [10].

When interpreting the plots of Figs. 1 and 2 it is useful to consider the position of the neutral Ce ground-state threshold, determined by subtracting the initial-state binding energy from the photon energy. The rest of the neutral spectrum is then placed at the appropriate energy difference moving toward the left (lower emitted electron energy). Alternatively, consider that as one moves up the rows of Figs. 1 and 2, the superimposed neutral spectrum is shifted to the right by the difference in the initial-state binding energies. For ease of comparison with the published neutral Ce spectrum [5], the *LS* designations presented therein are used in labelling the important neutral thresholds for each plot (our analysis, not shown, agrees in the leading terms in most cases).

Note that for the odd initial states, the plots are dominated by $4f5d^26s+\epsilon p$ channels. Since these channels represent $6s \rightarrow \epsilon p$, only channels with neutral thresholds with $J_{Ce} = J_{Ce^-} \pm 1/2$ have significant partial cross sections. In most cases, channels with moderate partial cross sections and neutral thresholds designated $4f5d6s^2$ [5] actually represent an interaction with the smaller amount of $4f5d^26s$ mixed into these thresholds. This is particularly important for ^3F and ^3G $4f5d6s^2$ levels where a small ($\sim$15%) amount of ^5H $4f5d^26s$ mixing results in partial cross sections in the 1.165-eV plots (where these channels are near threshold)

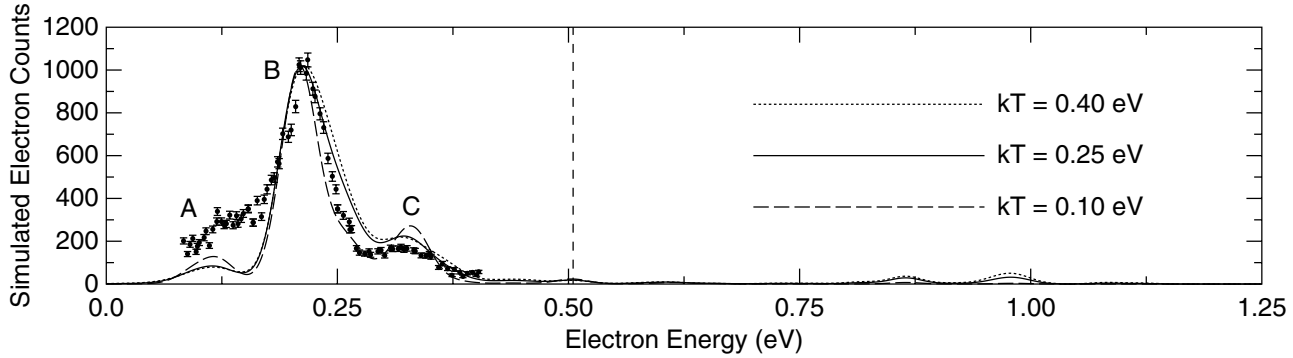

FIG. 4. Simulated electron counts for incident photon energy of 1.165 eV. The points and error bars are the Davis-Thompson [10] experimental results. The dashed vertical line indicates the position of the ground-state to ground-state channel with our revised interpretation.

roughly proportional to the amount of ^5H in those nearby $4f5d^26s$ levels. Also note that for transitions of the form $6s \rightarrow \epsilon p$ ($l=0 \rightarrow l=1$), the remaining portion of the negative-ion state must match the neutral threshold *LS*. For example, in the case of $^4I^o_{9/2}$ (binding energy 0.508 eV) the channel with the neutral $^3H^o_5$ threshold actually represents an interaction with the $^3I^o_5$ term mixed into this neutral Ce level. Finally, we note that an *LS* analysis more detailed than that of Table I indicates that the odd Ce^- $4f5d^26s^2$ states are primarily composed of basis functions whose $5d^2$ subgroup is restricted to ^3F, which explains the large partial cross sections with lower-lying thresholds with the same *LS* term of this subgroup [5]. Channels with neutral thresholds above $\sim 10\,000$ cm^{-1} have negligible partial cross sections due to $5d^2$ subgroups with terms of ^3P, ^1G, and ^1D [5], resulting in a lack of features in the odd Ce^- 2.410-eV photon plots below ~ 0.600 eV.

Photodetachment channels with odd initial states and neutral $4f5d6s^2$ thresholds (excluding those with $4f5d^26s$ mixing mentioned above) are found to have negligible partial cross sections with minimal contributions to the combined plots of Figs. 3 and 4. In particular we note that the combined $^4H_{7/2}$ channels with ^4H neutral thresholds ($^5H_3$ and $^5H_4$ are only separated by 69 cm^{-1}) produce a feature in the simulated spectrum ~ 35 times larger than the neutral $^1G_4$ ground-state channel. Since these transitions represent $5d \rightarrow \epsilon p$, the possibility of $\Delta J > 1/2$ between the negative-ion state and neutral threshold exists, but initial test calculations indicated such channels were several times smaller than those with $\Delta J = 1/2$. Also, we have made detailed calculations of $5d \rightarrow \epsilon f$ channels (only relevant to the $4f5d6s^2$ thresholds) for the lowest two odd Ce^- initial states, but these were found to also have negligible partial cross sections, of the same order as the corresponding ϵp channels to at most a few times larger than these partial cross sections. Since inclusion of such ϵf channels would have minimal impact on our final simulated plots of Figs. 3 and 4, we have refrained from further calculation of these partial cross sections.

The simulated electron count plots for the even Ce^- initial states are characterized by two separate features at low (<0.600 eV) and high (>2.000 eV) energy in the 2.410 eV photon plots. The low-energy features represent $6s \rightarrow \epsilon p$ channels with even neutral thresholds, either $4f5d6s6p$ levels or $4f^25d6s$ levels with significant $4f5d6s6p$ mixing (these thresholds begin above $\sim 13\,000$ cm^{-1} in the neutral Ce spectrum [5]). The high-energy features are produced by $6p \rightarrow \epsilon d + \epsilon s$ channels with $4f5d6s^2$ thresholds. As mentioned in Sec. II, interchannel coupling between these ϵd and ϵs channels has been neglected, with the separately calculated channels simply added together (the ϵd channels are generally 3–5 times larger). In principle, the inclusion of these channels in the final simulated plots should take into account a differing asymmetry parameter β for these channels, as well as the 45° declination angle of the original experiment [10]. However, upon noticing that these features are essentially "lost in the noise" of Fig. 3, we have declined to include separate estimated coefficients for them when generating these plots. Test calculations for these ϵd channels with Ce^- states and neutral thresholds with $\Delta J > 1/2$ were also found to have minimal contributions to our simulated plots.

With our revised interpretation of the experimental data [10], some of the features of Fig. 3 can now be better understood. The narrow peak 3, formerly identified with the ground-state to ground-state channel [10], can now be seen as a superposition of $^4H \rightarrow {}^5H + \epsilon p$ and $^4I \rightarrow {}^5I + \epsilon p$ channels. Note that both the ^5H and ^5I neutral thresholds increase in energy with increasing J [5] (the $^3G_5$ level at 3211 cm^{-1} should be considered as $^5H_5$ for this discussion as it has a significant mixing of ^5H and no other level has been designated as such for $J=5$ in the *LS* analysis [5]). A similar decrease of binding energy of similar size (~ 0.100 eV) with increasing J in the Ce^- $4f5d^26s^24\,{}^4H$ and ^4I states results in a nearly constant negative-ion and neutral-threshold energy difference for these partial cross sections, as evidenced by the consistency of the position of a peak in the 2.410-eV photon energy plots just below 1.500 eV (see Fig. 3).

The double feature of peak 2 of Fig. 3 is primarily due to the 0.110-eV difference in binding energy of two lowest odd Ce^- states and the large cross section of the channels representing transitions of both of these initial states to the same $^3H_4$ threshold. The full peak 2 feature is broader than peak 1 because there are two $4f5d^26s3\,{}^3H$ or ^3I basis functions with $^3F\ 5d^2$ subgroups for each J mixing over a wider range of neutral Ce levels [5] (^5H and ^5I each have one basis function per J). Similarly, the even $4f5d6s6p$ triplet (and quintet) terms also mix over a wide range of $4f5d6s6p$ and $4f^25d6s$ thresholds, producing the somewhat broader feature of peak 1.

In Fig. 4 there is some ambiguity in matching up the relative height of peaks. For example, we have normalized our simulated plots to match the height of peak *B*, but we have not added a constant background count which might increase the discrepancy between the experimental data [10] and our peak *C*. Regardless of vertical offset of the data, however, our peak *A* is significantly below the experimental data. The error here is perhaps due to difficulties of proper mixing of $4f5d^26s$ into certain $4f5d6s^2$ neutral Ce levels as discussed in Sec. II. Photodetachment partial-cross-section calculations made prior to the shifting of *LS* terms on the neutral Ce RCI calculations show the importance of these final adjustments to the RCI wave functions. In general, prior to these diagonal energy shifts the $4f5d6s^2$ triplet levels below the $4f5d^26s\,{}^5H$ levels had too much ^5H mixing and those triplet levels above ^5H had too little. A plot similar to Fig. 4 made at this stage would have a much larger peak *C* and a nearly nonexistent peak *A*. While further shifting of diagonal elements might improve our agreement with experiment [10], the simulated plots we have presented here are those for which our RCI level analysis best matches the experimental [5] Landé g values.

Finally, in Table III we present the largest $E1$ f values for the bound states of Ce^-. These data are not required in the above analysis used to determine binding energies, but we include them here as a correction to the corresponding table in our earlier work [9]. Regrettably, a clerical error resulted in those f values being presented 100 times larger than they should have been. Changes in the relative position of the $4f5d^26s^2$ and $4f5d6s^26p$ also result in large differences in these f values from the earlier tabulation. Note that these data, along with $M1$ and $E2$ f values not shown here, result

TABLE III. Largest Ce^- $E1$ f values (Babuskin gauge).

Transition	f value	Transition	f value	Transition	f value
$^4H^o_{7/2} \rightarrow {}^4G^e_{5/2}$	4.39×10^{-4}	$^2G^o_{7/2} \rightarrow {}^2G^e_{7/2}$	2.08×10^{-5}	$^2F^o_{5/2} \rightarrow {}^2D^e_{3/2}$	3.42×10^{-5}
$\rightarrow {}^2G^e_{7/2}$	1.39×10^{-4}	$\rightarrow {}^4H^e_{7/2}$	4.02×10^{-4}	$\rightarrow {}^2G^e_{7/2}$	9.50×10^{-5}
$\rightarrow {}^4H^e_{7/2}$	3.02×10^{-3}	$\rightarrow {}^2H^e_{9/2}$	6.62×10^{-4}	$\rightarrow {}^4H^e_{7/2}$	1.03×10^{-4}
$\rightarrow {}^2H^e_{9/2}$	3.57×10^{-4}	$\rightarrow {}^4I^e_{9/2}$	4.62×10^{-4}	$^2F^o_{7/2} \rightarrow {}^2G^e_{7/2}$	8.67×10^{-5}
$\rightarrow {}^4I^e_{9/2}$	1.00×10^{-4}	$^4H^o_{11/2} \rightarrow {}^4I^e_{9/2}$	8.58×10^{-4}	$\rightarrow {}^4H^e_{7/2}$	4.69×10^{-5}
$^4H^o_{9/2} \rightarrow {}^2G^e_{7/2}$	2.82×10^{-4}	$\rightarrow {}^2H^e_{11/2}$	3.82×10^{-5}	$\rightarrow {}^4I^e_{9/2}$	9.21×10^{-5}
$\rightarrow {}^4H^e_{7/2}$	7.74×10^{-4}	$^2G^o_{9/2} \rightarrow {}^2G^e_{7/2}$	5.09×10^{-5}	$^4D^o_{3/2} \rightarrow {}^2D^e_{3/2}$	4.54×10^{-3}
$\rightarrow {}^2H^e_{9/2}$	3.22×10^{-4}	$\rightarrow {}^2H^e_{9/2}$	2.55×10^{-5}	$^4I^o_{13/2} \rightarrow {}^2H^e_{11/2}$	5.35×10^{-4}
$\rightarrow {}^4I^e_{9/2}$	7.13×10^{-4}	$\rightarrow {}^4I^e_{9/2}$	6.34×10^{-4}	$^2G^e_{7/2} \rightarrow {}^4D^o_{5/2}$	4.78×10^{-5}
$\rightarrow {}^2H^e_{11/2}$	7.30×10^{-3}	$\rightarrow {}^2H^e_{11/2}$	1.76×10^{-4}	$\rightarrow {}^2H^o_{9/2}$	5.22×10^{-5}
$^4I^o_{9/2} \rightarrow {}^2G^e_{7/2}$	5.11×10^{-4}	$^4I^o_{11/2} \rightarrow {}^4I^e_{9/2}$	4.57×10^{-5}	$^2G^e_{5/2} \rightarrow {}^4F^o_{3/2}$	3.88×10^{-5}
$\rightarrow {}^4H^e_{7/2}$	9.27×10^{-4}	$\rightarrow {}^2H^e_{11/2}$	4.21×10^{-4}	$^2D^e_{3/2} \rightarrow {}^2S^o_{1/2}$	7.27×10^{-5}
$\rightarrow {}^4H^e_{9/2}$	2.34×10^{-4}	$^4H^o_{13/2} \rightarrow {}^2H^e_{11/2}$	4.35×10^{-4}	$\rightarrow {}^4F^o_{3/2}$	1.16×10^{-4}
$\rightarrow {}^4I^e_{9/2}$	7.64×10^{-4}	$^4D^o_{1/2} \rightarrow {}^2D^e_{3/2}$	2.17×10^{-3}	$^2H^o_{9/2} \rightarrow {}^4I^e_{9/2}$	3.95×10^{-5}
$\rightarrow {}^2H^e_{11/2}$	1.49×10^{-5}	$^2H^e_{9/2} \rightarrow {}^2H^o_{9/2}$	4.21×10^{-3}	$^4H^e_{7/2} \rightarrow {}^4F^o_{5/2}$	3.35×10^{-5}

in the lifetimes presented in Tables I and II. The bound states in Table III are labeled by the leading *LS* term, so some transitions appear forbidden due to differing total spin, but these represent interaction with a secondary *LS* term in the initial or final state (see Tables I and II).

IV. CONCLUSION AND FUTURE WORK

We believe these calculations are a significant improvement over past Ce^- calculations [4,9,11] and represent a greater understanding of the negative-ion states and their relation to their neutral Ce thresholds. The approach of using experimental energies [10] in conjunction with detailed computational analysis has served to resolve the various discrepancies concerning the Ce^- electron affinity that have existed now for over a decade. We expect that more recent experiments involving both LPES [21] and LPT [22] techniques will serve to confirm our estimate of the Ce^- electron affinity of approximately 0.660 eV. In particular, the focus on identification of the l of the emitted photoelectron in these experiments [21,22] will prove useful in this comparison with computed partial cross sections.

Due to the process of identifying dominant photodetachment channels, which involves ratios of partial cross sections of an order of magnitude or more in this case, this method is quite robust and forgiving to reasonably large errors in calculated cross sections. Even so, our methodology requires improvement to allow for possible future cases where interchannel coupling, careful treatment of resonances, and comparison to LPT experiments may be of more immediate concern.

ACKNOWLEDGMENT

Support from the National Science Foundation, Grant No. PHY-0097111, is gratefully acknowledged.

[1] M. A. Garwan, A. E. Lietherland, M. J. Nadeau, and X. L. Zhao, Nucl. Instrum. Methods Phys. Res. B **79**, 631 (1993).
[2] D. Berkovits, E. Obaretto, M. Paul, and G. Hollos, Rev. Sci. Instrum. **63**, 2825 (1992).
[3] S. H. Vosko, J. B. Lagowski, I. L. Mayer, and J. A. Chevary, Phys. Rev. A **43**, 6389 (1991).
[4] K. Dinov, D. R. Beck, and D. Datta, Phys. Rev. A **50**, 1144 (1994).
[5] *Atomic Energy Levels—The Rare-Earth Elements*, edited by W. C. Martin, R. Zalubas, and L. Hagan, Natl. Bur. Stand. Ref. Data Ser. Natl. Bur. Stand. (U.S.) Circ. No. 60 (U.S. GPO, Washington, D.C., 1978).
[6] D. Berkovits, S. Ghelberg, O. Heber, and M. Paul, Nucl. Instrum. Methods Phys. Res. B **123**, 521 (1997).
[7] A. M. Covington, D. Calabresse, J. S. Thompson, and T. J. Kvale, J. Phys. B **31**, L855 (1998).
[8] S. M. O'Malley and D. R. Beck, Phys. Rev. A **60**, 2558 (1999).
[9] S. M. O'Malley and D. R. Beck, Phys. Rev. A **61**, 034501 (2000).
[10] V. T. Davis and J. S. Thompson, Phys. Rev. Lett. **88**, 073003 (2002).
[11] X. Cao and M. Dolg, Phys. Rev. A **69**, 042508 (2004).
[12] V. T. Davis and J. S. Thompson, Phys. Rev. A **65**, 010501(R) (2001).
[13] V. T. Davis and J. S. Thompson, J. Phys. B **35**, L11 (2002).
[14] V. T. Davis and J. S. Thompson, J. Phys. B **37**, 1961 (2004).
[15] J. P. Desclaux, Comput. Phys. Commun. **9**, 31 (1975).

[16] P. G. Burke and K. A. Berrington, *Atomic and Molecular Process: An R-matrix Approach* (Institute of Physics, Bristol, 1993).
[17] K. A. Berrington, W. Eissner, and P. N. Norrington, Comput. Phys. Commun. **92**, 290 (1995).
[18] H. L. Zhou, S. T. Manson, A. Hibbert, L. V. Ky, N. Feautrier, and J.-C. Chang, Phys. Rev. A **70**, 022713 (2004).
[19] W. F. Perger, Z. Halabuka, and D. Trautmann, Comput. Phys. Commun. **76**, 250 (1993).
[20] M. G. Tews and W. F. Perger, Comput. Phys. Commun. **141**, 205 (2001).
[21] S. S. Duvvuri, R. G. Kraus, E. D. Emmons, J. S. Thompson, V. T. Davis, and A. M. Covington, Bull. Am. Phys. Soc. **51**, 154 (2006), and personal communication with the authors.
[22] C. W. Walter, N. D. Gibson, K. A. Starr, C. M. Janczak, D. A. Richardson, and P. Andersson, Bull. Am. Phys. Soc. **51**, 150 (2006), and personal communication with the authors.